

ATBD of GCOM-C ocean color atmospheric correction

Hiroshi Murakami (JAXA/EORC)

1. Introduction

GCOM-C/SGLI ocean color atmospheric correction algorithm applicable for the global ocean is developed (Fig. 1). The method is basically same as the general atmospheric correction algorithms developed for OCTS, SeaWiFS, MODIS, VIIRS, and so on (Gordon and Wang, 1994; Fukushima et al., 2002); normalized water-leaving radiance $nLw(\lambda)$ or remote sensing reflectance $R_{rs}(\lambda)$ is derived by using multiple channel (λ) observations. It is designed as a fast and small data lack algorithm because SGLI has 250-m spatial resolution and relatively narrow swath of 1150 km.

2. Method

Satellite observed reflectance, $\rho_t(\lambda)$, is calculated from $L_t(\lambda)$ by the following equation (1).

$$\rho_t(\lambda) = L_t(\lambda) \cdot \pi \cdot d^2 / F_0(\lambda) / \cos(\theta_s), \quad (1)$$

where F_0 is solar irradiance (see Table 1), d , ratio of solar-earth distance to the yearly average distance, θ_s , solar zenith angle.

Table 1 Center wavelengths, band weighted solar irradiance, and refractive index of SGLI channels

Channel	VN01	VN02	VN03	VN04	VN05	VN06	VN07	VN08	VN09	VN10	VN11	SW01	SW02	SW03	SW04
λ (nm)	380.03	412.51	443.24	489.85	529.64	566.15	672.00	672.10	763.07	866.76	867.12	1054.99	1385.35	1634.51	2209.48
F_0 (W/m ² /μm)	1092.14	1712.17	1898.32	1938.46	1850.96	1797.14	1502.55	1502.30	1245.45	956.34	956.62	646.54	361.24	237.58	84.25
Refractive index	1.3395	1.3383	1.3371	1.3351	1.3336	1.3327	1.3310	1.3310	1.3298	1.3287	1.3287	1.3267	1.3211	1.3168	1.2953

$\rho_t(\lambda)$ is approximated as following equation (2).

$$\rho_t(\lambda) / t_g(\lambda) = \rho_r(\lambda) + T(\lambda) \cdot \rho_g(\lambda) + \rho_a(\lambda) + \rho_w(\lambda) \cdot t(\lambda) / (1 - s_a(\lambda) \cdot \rho_w(\lambda)), \quad (2)$$

where ρ_r is Rayleigh scattering reflectance, ρ_a , aerosol reflectance, ρ_w , water-leaving reflectance, T , direct transmittance of sun-surface-satellite, t , direct + diffuse transmittance, s_a , spherical albedo, ρ_g , sun-glint reflectance, t_g , correction factor for water vapor, ozone, and oxygen absorption (Table 2). The white cap term is omitted in the eq. (2), because the spectral shape is similar with ρ_a and it can be corrected as a part of $\rho_a(\lambda)$.

Water-leaving reflectance ρ_w is derived by the eq. (3).

$$\rho_w(\lambda) = \rho_{aw}(\lambda) / (t(\lambda) + \rho_{aw}(\lambda) \cdot s_a(\lambda)), \quad (3)$$

Where,

$$\rho_{aw}(\lambda) = \rho_t(\lambda) / t_g(\lambda) - \rho_r(\lambda) - T(\lambda) \cdot \rho_g(\lambda) - \rho_a(\lambda). \quad (4)$$

$s_a \cdot \rho_w$ can be omitted because ρ_w of the ocean and s_a of the clear sky are generally small.

$R_{rs}(\lambda)$ and $nLw(\lambda)$ are derived by correcting directional dependency of in-water and sea-surface reflectance by LUT (R) (eq. (5) and (6)) developed and distributed by Morel and Maritorena 2001.

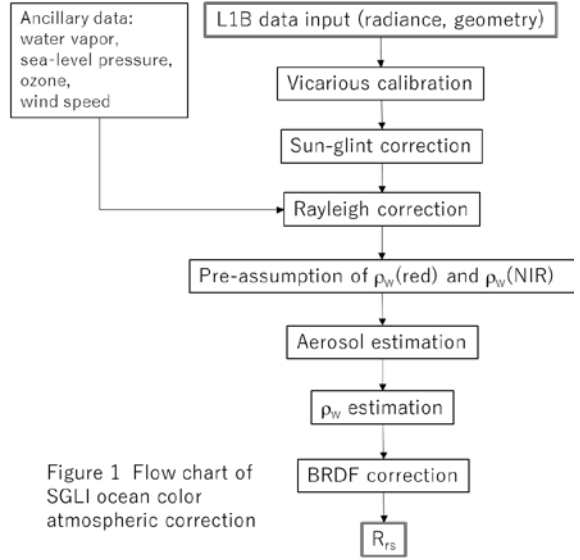


Figure 1 Flow chart of SGLI ocean color atmospheric correction

$$R_{rs}(\lambda) = (\rho_w(\lambda) / \pi) \cdot R(\theta=0, \theta_s=0, \Delta\phi, W, \text{Chl}, \lambda) / R(\theta, \theta_s, \Delta\phi, W, \text{Chl}, \lambda) \quad (5)$$

$$nLw(\lambda) = R_{rs}(\lambda) \cdot F_0(\lambda) \quad (6)$$

where θ is solar zenith angle, θ_s , solar zenith angle, $\Delta\phi$, relative azimuth angle, W , wind speed, and Chl , chlorophyll-a concentration.

Table 2 coefficients for gas absorption correction

gas	Channel	a	b	c
Vapor mm	VN01	1.4909E-06	0.0000E+00	0.00
	VN02	9.8080E-07	0.0000E+00	0.00
	VN03	3.1745E-05	0.0000E+00	0.00
	VN04	1.0449E-05	0.0000E+00	0.00
	VN05	1.6566E-05	0.0000E+00	0.00
	VN06	1.2198E-04	0.0000E+00	0.00
	VN07	5.6657E-05	0.0000E+00	0.00
	VN08	5.5299E-05	0.0000E+00	0.00
	VN09	1.6525E-06	0.0000E+00	0.00
	VN10	8.0907E-05	0.0000E+00	0.00
	VN11	7.5751E-05	0.0000E+00	0.00
	SW01	4.0931E-05	0.0000E+00	0.00
	SW02	-2.5585E-01	1.4719E+00	-0.32
	SW03	4.3975E-03	-2.8813E-03	0.06
SW04	1.7986E-02	-1.1061E-02	0.08	
Oxygen (sea-level pressure ratio)	VN01	1.6250e-03	0.0000e+00	0.00
	VN02	4.2290e-05	0.0000e+00	0.00
	VN03	4.7086e-04	0.0000e+00	0.00
	VN04	2.0450e-04	0.0000e+00	0.00
	VN05	1.1597e-03	0.0000e+00	0.00
	VN06	5.5712e-03	0.0000e+00	0.00
	VN07	1.9591e-03	-5.1393e-04	1.00
	VN08	2.0069e-03	-5.2653e-04	1.00
	VN09	3.1756e-02	2.8606e-01	-0.60
	VN10	4.4504e-05	0.0000e+00	0.00
	VN11	4.5281e-05	0.0000e+00	0.00
	SW01	8.5098e-03	0.0000e+00	0.00
	SW02	-7.1343E-04	9.0805e-04	1.00
	SW03	4.9989e-07	0.0000e+00	0.00
SW04	6.5526e-08	0.0000e+00	0.00	
Ozone DU	VN01	8.2534e-09	0.0000e+00	0.00
	VN02	2.5426e-07	0.0000e+00	0.00
	VN03	3.0227e-06	0.0000e+00	0.00
	VN04	2.0641e-05	0.0000e+00	0.00
	VN05	6.5554e-05	0.0000e+00	0.00
	VN06	1.1461e-04	0.0000e+00	0.00
	VN07	4.2756e-05	0.0000e+00	0.00
	VN08	4.2661e-05	0.0000e+00	0.00
	VN09	6.6933e-06	0.0000e+00	0.00
	VN10	1.9163e-06	0.0000e+00	0.00
	VN11	1.8778e-06	0.0000e+00	0.00
	SW01	8.0493e-08	0.0000e+00	0.00
SW02	3.5094e-09	0.0000e+00	0.00	

	SW03	0.0000e+00	0.0000e+00	0.00
	SW04	0.0000e+00	0.0000e+00	0.00

Look-up tables (LUTs) of $\rho_r(\lambda)$, $T(\lambda)$, $\rho_a(\lambda)$, $t(\lambda)$, and $s_a(\lambda)$ are calculated by Pstar4 (Ota et al., 2010; Nakajima and Tanaka, 1986; 1988; Stamnes et al., 1988) for possible solar and satellite geometries (θ , θ_s , $\Delta\phi$), aerosol optical thickness at 867nm (AOT), and aerosol types (M). The sea-surface Fresnel reflection is included in $\rho_r(\lambda)$.

Gas absorption correction, t_g in eq. (2) and (4) is calculated as followings.

$$t_g(\lambda) = t_{\text{vapor}}(\lambda) \cdot t_{\text{oxygen}}(\lambda) \cdot t_{\text{ozone}}(\lambda) \quad (7)$$

$$t_i(\lambda) = \exp(-(a_i(\lambda) + b_i(\lambda) \cdot (x_i \cdot \text{am})^{ci(\lambda)}) \cdot x_i \cdot \text{am}) \\ / \exp(-(a_i(\lambda) + b_i(\lambda) \cdot (\text{xnorm}_i \cdot \text{am})^{ci(\lambda)}) \cdot \text{xnorm}_i \cdot \text{am}) \quad (8)$$

where, x_i = vapor (H_2O), oxygen (O_2), and ozone (O_3), normal values of the gases, $\text{xnorm}_{i=\text{vapor}} = 14.186$ mm, $\text{xnorm}_{i=\text{oxygen}} = 1.0$, $\text{xnorm}_{i=\text{ozone}} = 343.79$ DU, $\text{am} = 1/\cos(\theta_s) + 1/\cos(\theta)$.

Oxygen volume, $x_{i=\text{oxygen}}$, is described as ratio of sea-level pressure to nominal sea-level pressure assuming oxygen ratio to the atmosphere is constant.

3. Aerosol model

Aerosol models (size distribution and refractive index) are designed based on AERONET climatology (Holben et al., 2001) and calculated by Pstar4. Volume size distribution, V , is modeled by the eq. (9).

$$V = \exp((\ln(R/\text{RM})/\ln(S))^2 / 2) \quad (9)$$

R indicates particle size, (μm), RM , mode radius, and S , deviation. Ninth candidate models are made by mixing the fine mode and the coarse mode aerosols with fine mode ratio = 100, 68, 45, 29, 18, 11, 6, 3, and 0 %.

Fig. 2 shows an example of $\rho_a(\lambda)$ and $t(\lambda)$ of the ninth aerosol types. They are normalized by aerosol reflectance at the aerosol correction base channel, VN11 (867nm).

Table 3 size distribution parameters and refractive index

	RM (μm)	S	kr	ki
Fine	0.143	1.537	1.439	1.000E-08
Coase	2.59	2.054	1.363	3.000E-09

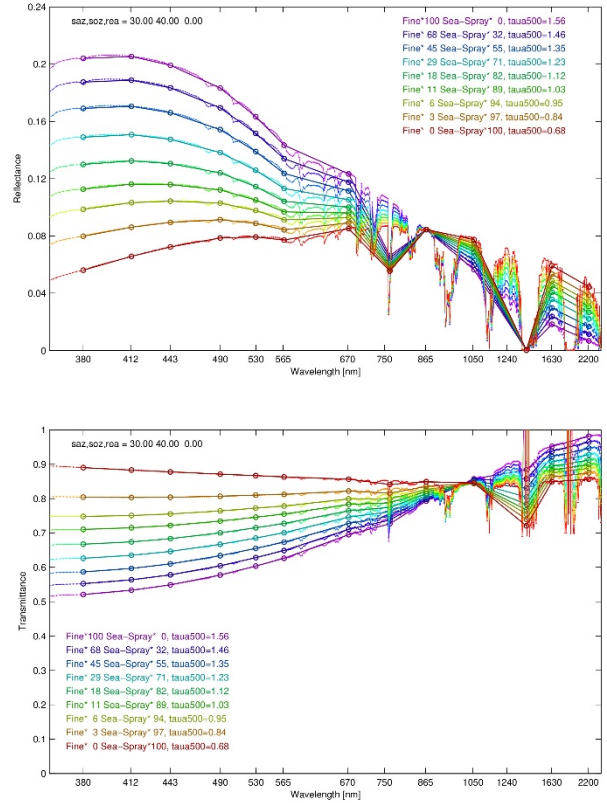


Figure 2 Aerosol reflectance and transmittance calculated by Pstar4

4. Sun-glint correction

Sun-glint reflectance, ρ_g , is calculated using objective analysis wind speed, W , by Cox and Munk (1954) (eq.10). T of AOT=0.3 is used to reduce the amount of the correction and avoid data lack by the over correction

$$\rho_g = \rho_w (1 - 2 m \cdot y \cdot z \cdot \cos_w), \quad (10)$$

$$\rho_w = \exp(-\tan(\theta)^2/s)/s/(4 \text{cth0} \cdot \text{cth} \cdot \cos(\theta)^4),$$

$$y = \sqrt{m^2 + \cos_w^2 - 1} / m,$$

$$z = 1 / (\cos_w + y \cdot m)^2 + 1 / (y + m \cdot \cos_w)^2,$$

$$\cos_w = \cos(\text{acos}(\text{cth} \cdot \text{cth0} + \text{sth} \cdot \text{sth0} \cdot \text{cdp})/2),$$

m : refractive index of the sea water (see Table 1),

$$\theta = \text{acos}((\text{cth} + \text{cth0}) / (2 \cos_w)),$$

$$s = 0.003 + 0.00512 W,$$

where, $\text{sth0} = \sin(\theta_0)$, $\text{cth0} = \cos(\theta_0)$, $\text{sth} = \sin(\theta)$, $\text{cth} = \cos(\theta)$, $\text{cdp} = \cos(\Delta\phi)$.

5. First guess of water-leaving reflectance

ρ_w at Near-infrared (VN10) and red (VN07) channels are pre-assumed for the aerosol estimation. Empirical relation of ρ_w to Liner Combination Index (Frouin et al., 2006) (I_{LC} in eq. (11)) is constructed by an inherent optical property (IOP) model based on NOMAD (Werdell and Bailey 2005) (eq. 12.1-2).

$$I_{LC} = \rho_w(\text{VN04}) - 1.4239 \rho_w(\text{VN06}) + 0.4104 \rho_w(\text{VN10}) \quad (11)$$

$$\rho_w^{\text{pre}} = (c_{L0} + c_{L1} I_{LC} + c_{L2} I_{LC}^2) \cdot \pi \quad (I_{LC} < 0.003), \quad (12.1)$$

$$\rho_w^{\text{pre}} = (c_{H0} + c_{H1} I_{LC} + c_{H2} I_{LC}^2) \cdot \pi \quad (I_{LC} \geq 0.003). \quad (12.2)$$

Eq. (11) can be applied to ρ_w derived by eqs. (3) and (4) without aerosol because I_{LC} is not sensitive to aerosols (Frouin et al., 2006). The coefficients of eqs. (12-1,2) are shown in Table 4.

Table 4 Coefficients for pre-estimation of ρ_w

λ	c_{L0}	c_{L1}	c_{L2}	c_{H0}	c_{H1}	c_{H2}
VN07	0.00057	-0.04968	0.75074	0.00057	-0.04968	0.75074
VN10	0.00005	-0.00935	0.36803	0.00005	-0.00935	0.36803

6. Aerosol optical thickness and model selection

AOT and M ($M_{i=1-9}$) are selected by searching a condition that the observed left hand is agree with the Pstar simulated right hand in eq. (13).

$$\rho_t(\lambda) / t_g(\lambda) \rho_r(\lambda) - T(\lambda) \cdot \rho_g(\lambda) = \rho_a(\lambda) + \rho_w^{\text{pre}}(\lambda) \cdot t(\lambda) / (1 - s_a(\lambda) \cdot \rho_w^{\text{pre}}(\lambda)), \quad (13)$$

Practically, AOT is selected by eq. (13) using observation and simulation at VN10 for each M firstly, and an optimal M is selected by observation and simulation at VN07.

If ρ_w at visible channels (VN02-VN05) become negative by the selected M , it is re-selected by assuming the blue channel ρ_w is zero.

7. Vicarious calibration

The ocean color estimation requires 0.2-0.3% accuracy of the inter-band relative calibration, even though the error of pre-launch characterization and on-orbit calibration can reach to 2-3%. The inter-band calibration (adjustment) can be conducted by using in-situ R_{rs} and the ocean color atmospheric correction LUTs. The temporal change is estimated by post-launch moon calibration, and the results will be reflected in the SGLI Ver.2 calibrated radiance data (LIB data).

$$L_{LIB}(\lambda) = L_{orig}(\lambda) / (1.0 + kt(\lambda) D) \quad (14)$$

where D indicates days from 00:00 1st Jan 2018(=0). $kt(\lambda)$ is shown in Table 5.

R_{rs} of MOBY (Clark et al., 2003) and BOUSSOLE (Antoine et al., 2006) are used as the vicarious calibration standard in multiple satellite missions. The coefficients, $k_0(\lambda)$, are derived by Murakami et al., 2005 (Table 5, Fig. 3). $L_{corr}(\lambda)$ in eq. (15) is used as $L_t(\lambda)$ in eq. (1).

$$L_{corr}(\lambda) = L_{LIB}(\lambda) / k_0(\lambda) \quad (15)$$

The MOBY +BOUSSOLE result in Table 5 is used for the SGLI ver. 2 ocean color processing.

Table 5 SGLI Vicarious calibration coefficients

Channel	VN01	VN02	VN03	VN04	VN05	VN06	VN07	VN08	VN09	VN10	VN11
kt (day ⁻¹)	-6.20E-5	-6.06E-5	-5.79E-5	-5.05E-5	-4.20E-5	-3.06E-5	-5.04E-6	-4.34E-6	0.0	0.0	0.0
k0 (MOBY +BOUSSOLE N=72)*	0.976	1.023	0.997	1.015	1.051	1.033	1	1.002	0.998	1	1
k0 (MOBY N=55)	0.982	1.029	1.003	1.019	1.056	1.036	1	1.003	1.017	1	1
k0 (BOUSSOLE N=17)	0.954	0.999	0.977	1.001	1.036	1.026	1	0.996	0.945	1	1

* recommended for the ocean color processing

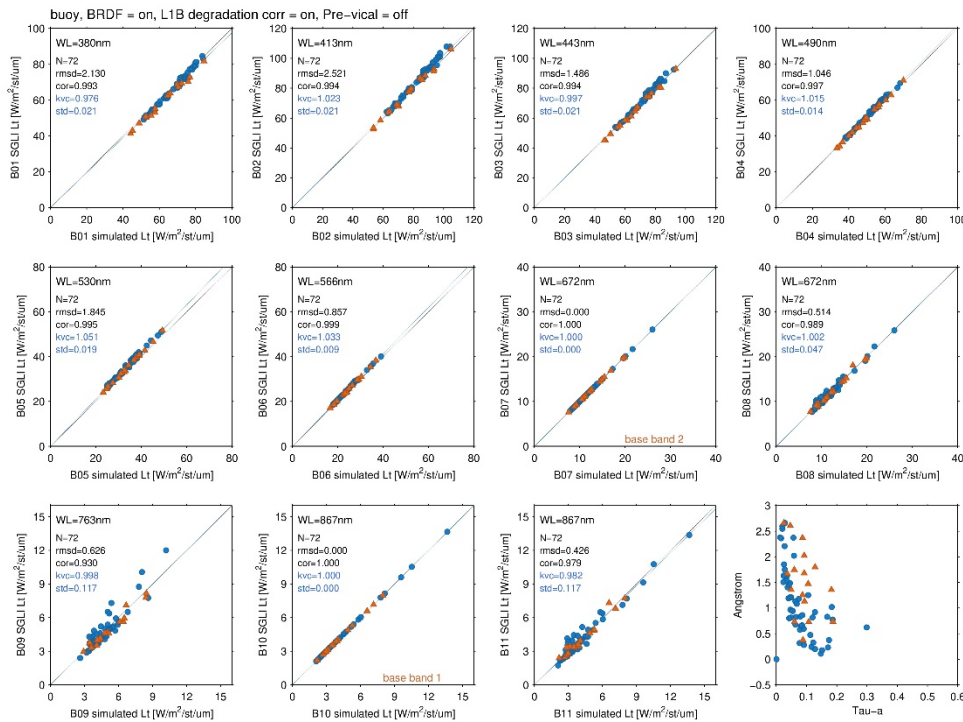


Figure 3 SGLI Vicarious calibration by MOBY and BOUSSOLE
Blue dots indicate MOBY samples, and red, BOUSSOLE samples

8. QA_flag

The first 0-1 bits are common for the Level-2 products, input data lack and land/water flags. Others are defined as the right table.

Cloud masks are set by the Rayleigh corrected reflectance of blue, red and near-infrared channels, and the near cloud is set by the maximum or deviation of the 5x5 pixel reflectance. Dark pixel is set when water-leaving reflectance of VN06<0.002. Case-2 flag is set if water-leaving reflectance of VN07>0.008 and Chl-a>60mg/m³.

The Level-3 statistics processing will input data when the bits of QA_flag indicated in Table 6 are not set and the product value is within the valid range

Table 6 Bit specification of QA_flag

bit	Description	L3 mask (NWLRL)	L3 mask (PAR)	L3 mask (FAI)
0	no observation data	1	1	1
1	land (0: ocean, 1: land)	1	1	1
2	incomplete VNR bands	1	1	1
3	cloud or ice	1	0	1
4	near cloud (+-2pix)	1	0	1
5	dark pixel	0	0	0
6	coast pixel	0	0	1
7	straylight flag	0	0	0
8	sunlint mask>0.16	0	0	0
9	sunlint flag>0.01	0	0	0
10	wind speed>20m/s	0	0	0
11	soz>75	0	0	0
12	taua>0.5	0	0	0
13	out of aerosol models;	0	0	0
14	negative nLw	0	0	0
15	turbid Case-2 water	0	0	0

Reference

- Gordon, H. R., and M. Wang (1994), "Retrieval of water-leaving radiance and aerosol optical thickness over the oceans with SeaWiFS: a preliminary algorithm," *Appl. Opt.* **33** (3), 443-452.
- Fukushima, H., and R. Frouin, 2002: GLI algorithm description (ATBD), Atmospheric Correction for Ocean Color: <http://suzaku.eorc.jaxa.jp/GLI/ocean/algorithm/index.html>.
- Morel, A., and S. Maritorena (2001), "Bio-optical properties of oceanic waters: A reappraisal," *J. Geophys. Res.*, 106, C4, 7163-7180.
- Ota, Y., A. Higurashi, T. Nakajima, and T. Yokota (2010), "Matrix formulations of radiative transfer including the polarization effect in a coupled atmosphere-ocean system," *J. Quantitative Spectroscopy and Radiative Transfer*, **111**, 878-894.
- Nakajima, T., and M. Tanaka (1986), "Matrix formulation for the transfer of solar radiation in a plane-parallel scattering atmosphere," *J. Quantitative Spectroscopic Radiative Transfer*, **35**, 13-21.
- Nakajima, T., and M. Tanaka (1988), "Algorithms for radiative intensity calculations in moderately thick atmospheres using a truncation approximation," *J. Quantitative Spectroscopic Radiative Transfer*, **40**, 51-69.
- Stamnes, K., S.-C. Tsay, W. Wiscombe, and K. Jayaweera (1988), "Numerically stable algorithm for discrete-ordinate-method radiative transfer in multiple scattering and emitting layered media," *Appl. Opt.*, **27**, 2502-2509.
- Holben, BN, Tanré, D, Smirnov, A, Eck, TF, Slutsker, I, Abuhassan, N, Newcomb, WW, Schafer, JS, Chatenet, B, Lavenu, F, Kaufman, YJ, Vande Castle, J, Setzer, A, Markham, B, Clark, D, Frouin, R, Halthore, R, Karneli, A, O'Neill, NT, Pietras, C, Pinker, RT, Voss, K & Zibordi, G 2001, 'An emerging ground-based aerosol climatology: Aerosol optical depth from AERONET', *J. Geophys. Res. C: Oceans*, vol. 106, no. D11, 2001JD900014, pp. 12067-12097.
- Murakami, H., M. Yoshida, K. Tanaka, H. Fukushima, M. Toratani, A. Tanaka, and Y. Senga, 2005: Vicarious calibration of ADEOS-2 GLI visible to shortwave infrared bands using global datasets, *IEEE Transactions on Geoscience and*

Remote Sensing, 43, 7, 1571-1584, 10.1109/TGRS.2005.848425.

Cox, C., and W. Munk, (1954), "Measurement of the roughness of the sea surface from photographs of the sun's glitter," J. Opt. Soc. Amer., vol. 44, pp. 838-850.

Werdell, P. J., and S.W. Bailey (2005), "An improved bio-optical data set for ocean color algorithm development and satellite data product validation," Remote Sens. Environment, 98, 122-140.

Frouin, R., Deschamps, P., Gross-Colzy, L. et al. , "Retrieval of chlorophyll-a concentration via linear combination of ADEOS-II Global Imager data", J. Oceanogr 62, 331-337 (2006) doi:10.1007/s10872-006-0058-2.

Clark, D. K., M. A. Yarbrough, M. Feinholz, S. Flora, W. Broenkow Y.-S. Kim, B. C. Johnson, S. W. Brown, M. Yuen, and J. L. Mueller, Chapter 2 MOBY, A Radiometric Buoy for Performance Monitoring and Vicarious Calibration of Satellite Ocean Color Sensors: Measurement and Data Analysis Protocols, Ocean Optics Protocols For Satellite Ocean Color Sensor Validation, Revision 4, Volume VI, 2003-0063145.

Antoine D, Chami M, Claustre H, D'Ortenzio F, Morel A, Bécu G, Gentili B, Louis F, Ras J, Roussier E, Scott AJ, Tailliez D, Hooker SB, Guevel P, J-F Desté, Dempsey C, Adams D (2006) BOUSSOLE : a joint CNRS-INSU, ESA, CNES and NASA Ocean Color Calibration And Validation Activity. NASA Technical memorandum No. 2006-214147, NASA/GSFC, Greenbelt, MD, 61 pp.

Murakami, H., M. Yoshida, K. Tanaka, H. Fukushima, M. Toratani, A. Tanaka, and Y. Senga, 2005: Vicarious calibration of ADEOS-2 GLI visible to shortwave infrared bands using global datasets, IEEE Transactions on Geoscience and Remote Sensing, 43, 7, 1571-1584, 10.1109/TGRS.2005.848425.